Application of Nonlinear Finite Element Analysis on Shear-Critical Reinforced Concrete Beams

Asdam Tambusay[1,2], Priyo Suprobo[1], Benny Suryanto[2,*] & Warren Don[2]

[1]Department of Civil Engineering, Faculty of Civil, Planning and Geo Engineering, Sepuluh Nopember Institute of Technology, Indonesia
[2]School of Energy, Geoscience, Infrastructure and Society, Institute for Infrastructure and Environment, Heriot-Watt University, Edinburgh, United Kingdom
*E-mail: B.Suryanto@hw.ac.uk

Highlights:

- Examples of user constitutive models in ATENA Science.
- Application of the smeared crack approach utilizing the crack and crush band methods.
- Detailed comparisons of load-deflection responses and failure modes of shear-critical reinforced concrete beams.
- Insights into computed crack patterns, principal tensile strains and failure mechanisms.
- Demonstration of a range of analysis capabilities for practicing engineers.

Abstract. This paper presents the application of a smeared fixed crack approach for nonlinear finite element analysis of shear-critical reinforced concrete beams. The experimental data was adopted from tests undertaken on twelve reinforced concrete beams by Bresler and Scordelis in 1963, and from duplicate tests undertaken by Vecchio and Shim in 2004. To this end, all beams were modeled in 3D using the software package ATENA-GiD. In the modeling, the nonlinear behaviors of the concrete were represented by fracture-plastic constitutive models, which were formulated within the smeared crack and crack/crush band approaches. The applicability of nonlinear analysis was demonstrated through accurate simulations of the full load-deflection responses, underlying mechanisms, crack patterns, and failure modes of all 24 beams. Detailed documentation of the results is presented to demonstrate the potential and practical value of nonlinear finite element analysis in providing an informed assessment of the safety and performance of reinforced concrete structures.

Keywords: *ATENA; GiD; nonlinear finite element; shear failure; smeared crack.*

1 Introduction

Accurate modeling of the nonlinear response of reinforced concrete has an important role to play in providing accurate predictions of the multifaceted nonlinear behavior of reinforced concrete structures. Although the response of reinforced concrete can be regarded as linear under normal loading conditions, it can become highly nonlinear when subjected to extreme loading conditions, for

example during a seismic event [1]. High nonlinearity can also occur when the load applied is considerably larger than the anticipated value, for example in poorly designed or constructed structures [2-4], or in structural elements with complex detailing [5-7]. In such situations, both the concrete and the reinforcing steel can contribute to the overall structural nonlinearity to a greater or lesser extent. In the case of the concrete, this is due to the complex behavior of cracked concrete, generally exhibiting the formation of cracks and opening/closing of pre-existing cracks [3,8], crack slip and shear transfer along crack interfaces [9,10], and crack-to-crack interactions [7].

Compared to concrete, reinforcing steel can be considered as a far more linear material. Under service load conditions, local variations in stresses and strains can be expected to develop along the steel embedded in the concrete due to concrete cracking, bond conditions, and dowel action [11,12]. When steel begins to yield, however, it can turn into a highly nonlinear material and exert a dominant influence on the overall structural response. This is due to the large deformation caused by the yielding of the steel reinforcement. While most welcome from a structural design point of view, due to the ductile response exhibited, this large deformation may cause further damage to the concrete and hence increase the complexity of the problem at hand. The purpose of modeling is to capture the key features of the highly complex behavior of reinforced concrete without resorting to all the details but still maintaining accuracy. This forms the basis for the smeared crack approach, which is well documented [13,14].

Situations may arise where the applied load causes damage mainly to the concrete, resulting in undesirable brittle failure without being preceded by yielding of the steel reinforcement. This can occur, for example, in beams that are overly reinforced [2,15], in beams with little or no shear reinforcement subjected to restraint-induced tensile forces [16], or in beams with a non-compliant bar spacing and/or arrangement [17,18]. Not only does failure of such members give little or no warning, the load (shear) capacity will also be difficult to predict with accuracy and it is generally less well understood by design engineers [19]. The latter can partly be attributed to the empirical nature of shear design code provisions, particularly for members without shear reinforcement. This is understandable, as unlike flexural behavior, which can be conveniently related to the section compatibility and equilibrium of compressive and tensile longitudinal forces, shear behavior and related mechanisms involve a more complicated problem over multiple sections.

Apart from design engineers, shear analysis of reinforced concrete members presents a major challenge to finite element modelers [20-22]. This can partly be attributed to the complex nature of the problem, generally involving non-uniform crack formation and a dominant crack that may have a major impact on the overall

structural response [23]. To address this issue, Vecchio & Shim [24] implemented a disturbed stress field formulated within the smeared crack approach. They used this approach to replicate the load-deflection response of twelve shear-critical reinforced concrete beams, reported previously by Bresler & Scordelis [25], and twelve duplicate beams [24]. These were specifically tested to investigate the post-peak ductility, in which reasonable agreements were reported based on the load-deflection responses and modes of failure. In their study, the importance of out-of-plane reinforcement in two-dimensional nonlinear finite element analysis of reinforced concrete beams with shear reinforcement was specifically highlighted. The reason for this was to account for the confinement effects introduced by the loading plate on the strength of the concrete in the vicinity of the plate. The use of a concrete tensile strength of $0.33\sqrt{f_c'}$ (MPa) is recommended to obtain a lower-bound prediction for beams with no shear reinforcement, considering the brittle nature of such beams [24]. The results of these classical beam tests and their duplicates have since been the subject of further studies and are generally used to benchmark the accuracy of nonlinear finite element procedures. This includes the work by Ceresa *et al.* [26], who employed several commercially available software packages; Ma [27] who incorporated a stochastic analysis to consider natural variations in material properties; and Bernard [28] who investigated the influence of corrosion on load capacity and the orientation of the principal concrete compressive stresses.

In this paper, the three-dimensional nonlinear finite element software ATENA Science was used to simulate the full load-deflection responses of Bresler and Scordelis beams [25] and their duplicates (Vecchio and Shim beams) [24]. All beams were simulated in 3D to avoid the use of additional assumptions (i.e. out-of-plane reinforcement and/or local increase in concrete strength) as in the previous work and to enable the analysis to be done in an objective manner. To this end, the smeared fixed crack approach was employed along with nonlinear constitutive models of concrete and steel, the details of which are presented below.

This paper focuses on providing researchers and practicing engineers with a better understanding of the shear mechanisms in reinforced concrete beams, knowledge that can be used to develop and further improve the provisions for the shear strength of such members. This paper also aims to demonstrate the potential of a simple, yet powerful tool that can be employed to provide a detailed and informed assessment of the safety and integrity of new or deteriorated reinforced concrete members, by researchers and structural engineers alike.

2 Details of Vecchio-Shim Beams

In 2004, Vecchio and Shim [24] undertook an experimental testing program on twelve shear-critical reinforced concrete beams, which were essentially identical to the beams tested by Bresler and Scordelis four decades earlier [25] (hereinafter referred to as VS and BS beams, respectively). The testing program aimed to verify the repeatability of the original experiment, particularly with respect to failure modes and load-bearing capacities, and to investigate the post-peak responses, which were not explored in the original experiment.

A schematic diagram of the beam geometry and reinforcement layout is displayed in Figure 1, with the beam cross-section details presented in Figure 2 and Table 1 for clarity. Four series of three beams were tested: the OA series with no transverse reinforcement; and the A, B, and C series, all containing transverse reinforcement. In each series, the beam was labeled with a numeral suffix to indicate the overall span: 1 representing a short span (3.66 m); 2 representing an intermediate span (4.57 m); and 3 representing a long span (6.40 m).

As summarized in Table 1, all beams had a rectangular cross-section and the same overall depth of 552 mm. In each series, the beam width, the amount of transverse reinforcement, and concrete strength were varied. The steel reinforcement used in the beam tests is listed in Table 2.
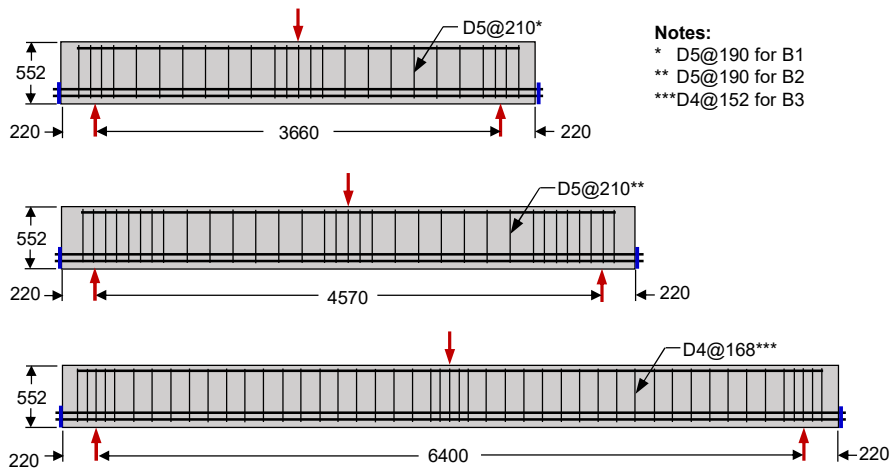

Figure 1 Geometric and reinforcement details of VS beams (adapted from [24]).
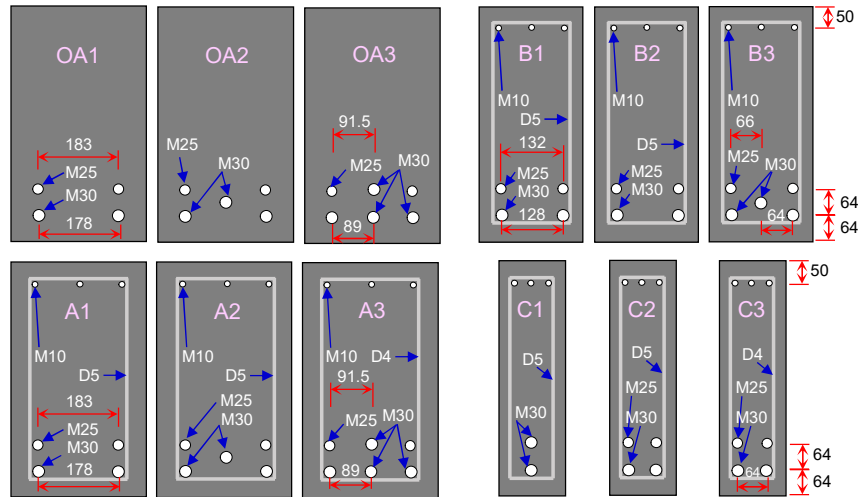
Figure 2 Cross-section details of VS beams (adapted from [24]).

Table 1 Cross-section of VS beams (unit dimension and length in mm) [24]

Beam	b	h	d	L	Span	Bottom Bar	Top Bar	Stirrup
OA1	305	552	457	4100	3660	2M30; 2M25	–	–
OA2	305	552	457	5010	4570	3M30; 2M25	–	–
OA3	305	552	457	6840	6400	4M30; 2M25	–	–
A1	305	552	457	4100	3660	2M30; 2M25	3M10	D5-210
A2	305	552	457	5010	4570	3M30; 2M25	3M10	D5-210
A3	305	552	457	6840	6400	4M30; 2M25	3M10	D4-168
B1	229	552	457	4100	3660	2M30; 2M25	3M10	D5-190
B2	229	552	457	5010	4570	2M30; 2M25	3M10	D5-190
B3	229	552	457	6840	6400	3M30; 2M25	3M10	D4-152
C1	152	552	457	4100	3660	2M30	3M10	D5-210
C2	152	552	457	5010	4570	2M30; 2M25	3M10	D5-210
C3	152	552	457	6840	6400	2M30; 2M25	3M10	D4-168

Table 2 Material properties of steel reinforcement in VS beams [24].

Bar Size	M10	M25[a]	M25[b]	M30	D4	D5
Diameter (mm)	11.3	25.2	25.2	29.9	3.7	6.4
f_y **(MPa)**	315	440	445	436	600	600
f_u **(MPa)**	460	615	680	700	651	649
E_s **(GPa)**	200	210	220	200	200	200

Note: [a] Series 2; [b] Series 1 and 3.

Table 3 presents the reported concrete properties for each series of beams. Only the compressive strength was considered in the analysis; all other properties were estimated using the default models in ATENA (discussed below).

Table 3 Material properties of concrete in VS beams (adapted from [24]).

Beam Label Suffix	f_c' (MPa)	ε_{cu} (%)	E_c (GPa)	f_t (MPa)
1	22.6	0.16	36.5	2.37
2	25.9	0.21	32.9	3.37
3	43.5	0.19	34.3	3.13

Steel plates with dimensions of $150 \times 350 \times 20$ mm and $150 \times 300 \times 58$ mm were used at both the support and loading points, respectively. This in addition to 25-mm thick end plates, which were welded to the bottom reinforcement at both ends of each beam to ensure adequate anchorage.

3 Nonlinear Finite Element Analysis

In this study, nonlinear finite element analysis was performed using the ATENA Science. ATENA is a user-friendly software package developed specifically by Červenka Consulting [29] for the analysis of reinforced concrete structures. In this software package, various nonlinear behaviors of reinforced concrete can be dealt with, including concrete cracking, reinforcement yielding, bonding between the concrete and the reinforcement, and concrete crushing under varying levels of confinement. Recent applications include simple flexural analysis [30], shear and punching failure analysis [31-33], beam-column joints under reversed cyclic loading [34], and durability assessment [35].

In ATENA Science, two fully integrated software packages are utilized, namely GiD and ATENA. The former is used as a pre-processor for defining the geometric and material properties, along with the generation of the finite element mesh. When a finite element model is run in GiD, it can be loaded automatically into either ATENA Console or ATENA Studio for performing nonlinear analysis. ATENA Studio was employed in this study, as it can also be used for post-processing the results. It has a unique visualization feature, which allows the results and progress of analyses such as load-deflection response, deformed shape, stress and strain conditions, and crack formation in the concrete to be viewed on screen in real-time while the analysis is still in progress.

Within ATENA's library, three smeared crack models are available: a fixed crack model, a fully rotating crack model, and a combination of both (by limiting the maximum residual tensile stress across a crack) [37]. Within the fixed crack formulation implemented in ATENA, up to a maximum of three cracks can be considered at each material point. This would mean that after the formation of the first crack, new cracks can still form at other inclinations if the stress conditions in the cracked concrete are governing. In this work, this type of crack representation was considered appropriate to represent cracked concrete in both

series of beams. Given that all BS and VS beams contain no or a low amount of transverse reinforcement, significant rotation of stress fields is expected but not to the extent that this would cause significant rotation in crack direction due to crack slips. This would be a good test for verifying the crack representation chosen above and the material models adopted in this paper (discussed below). The other two crack models available in the software library (i.e. rotating and hybrid) can also be employed to suit the problem at hand.

3.1   Compression and Tension Models

In ATENA, the nonlinear behavior of concrete is modeled using the fracture-plastic constitutive models for concrete [37]. The fracturing model is based on the model described in [40] and is used for representing the behavior of concrete in tension, whereas the plastic model is based on the work reported in [38] and is used for representing the behavior of concrete in compression under multiaxial stress conditions. The formulation of the material models is based on small strains, and strain decomposition into elastic, plastic, and fracturing components [35,37]. The stress development during the analysis is computed through an iterative algorithm, using rate equations that indicate progressive damage due to concrete cracking and plastic yielding caused by concrete crushing. For more details, the readers are referred to [35,37,39].

Several fracture-plastic models are available in the software library; two commonly adopted models are Cementitious2 and CementitiousUser. In the former model, the only input required is the cube compressive strength of concrete, which is used to determine the other parameters that are required for the analysis. Should it be necessary to modify some of the parameters, the second (user) model can be selected, as it gives users the flexibility to provide appropriate input data for the constitutive laws. The second model was employed in this study.

Figures 3(a) and (b) present the compression model employed in this study, with a parabolic shape representing the ascending (hardening) part and a linear shape representing the descending (softening) part. In the ascending part, the ratio of normal compressive stress σ_c (MPa) to the cylinder compressive strength f_c' (MPa) is related to the compressive stress beyond the elastic limit f_{co} (MPa), the equivalent concrete plastic strain ε_{eqp} (mm/mm), and the plastic strain at the peak stress ε_c^p (mm/mm) in the following manner [37,38]:

$$\frac{\sigma_c}{f_c'} = f_{co} + \left(f_c' - f_{co}\right)\sqrt{1 - \left(\frac{\varepsilon_{eqp} - \varepsilon_c^p}{\varepsilon_{eqp}}\right)^2} \qquad (1a)$$

$$\varepsilon_c^p = \frac{f_c'}{E_c} \tag{1b}$$

$$E_c = (6000 - 15.5 f_{cu})\sqrt{f_{cu}} \tag{1c}$$

$$f_{cu} = \frac{f_c'}{0.85} \tag{1d}$$

In Eq. (1a), the compressive stress beyond the elastic limit, f_{co}, is taken as twice the tensile strength of concrete ($= 2f_t$ MPa) [37]. The Young modulus of concrete E_c (MPa) is determined based on the cube compressive strength f_{cu} (MPa) (Eq. 1(c)); the relation between the cube and cylinder compressive strengths is provided in Eq. 1(d). This nonlinear hardening is part of the Menetrey-Willam model, which is used for representing the plasticity of concrete under multiaxial stress conditions. For the OA beam series with no shear reinforcement, the beta parameter in the plasticity model was taken as 0, whereas for the other beams it was taken as 0.5. For more details, the reader is referred to [35,37,40].
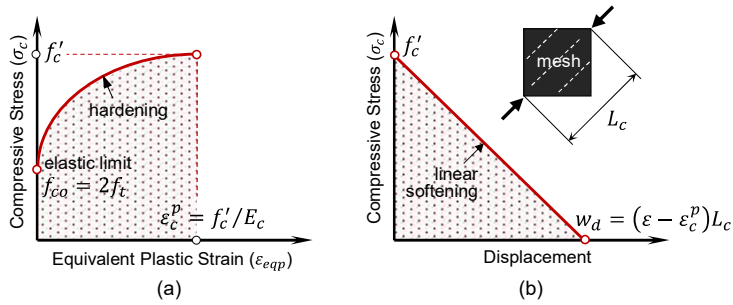

Figure 3 Compression model for concrete: (a) hardening and (b) softening [37].

While the ascending branch of the compression model is computed based on the strains, the descending (softening) branch is computed based on the displacement following the crush band approach to ensure mesh objectivity [37]. In this model, it is assumed that the post-peak compressive stress decreases linearly from the peak stress f_c' to zero stress at a prescribed displacement, w_d (see Fig. 3(b)). A value of $w_d = 2.5$ mm was adopted, following the recommendation by Červenka, *et al.* [39]. The crush band size L_c was calculated for each finite element mesh as the element size projected into the direction of the minimum compressive stress. Moreover, the mesh orientation bias was minimized using an orientation correction factor [37,39] and the minimum crush band size was taken as the minimum beam dimension to reduce the dependency of the results on mesh size [39].

In the tension (fracturing) model, the Rankine failure criterion was used for defining concrete cracking. In the fixed crack representation, stresses and strains

were computed in a local coordinate system in which the orientation was determined by the orientation of the principal stresses at the onset of cracking. Figure 4(a) displays a schematic of the post-cracking response of concrete, displaying a softening law that is formulated based on the crack opening displacement, w, and fracture energy, G_f. This is determined based on the fictitious crack band model and the experimentally derived empirical expressions proposed by Hordijk [40], as given by

$$\frac{\sigma_t}{f_t} = \left(1 + \left(c_1 \frac{w}{w_c}\right)^3\right) exp\left(-c_2 \frac{w}{w_c}\right) - \frac{w}{w_c}(1 + c_1{}^3)exp(-c_2) \tag{2a}$$

$$f_t = 0.24 f_{cu}^{\frac{2}{3}} \tag{2b}$$

$$w = \varepsilon_t L_t \tag{2c}$$

$$w_c = 5.14 \frac{G_f}{f_t} \tag{2d}$$

$$G_f = G_{f0} \left(\frac{f_c'}{10}\right)^{0.7} \tag{2e}$$

where σ_t is the tensile stress (MPa); f_t is the concrete tensile strength (MPa); w is the crack opening displacement (mm); w_c is the crack opening at the complete release of stress (mm); L_t is the characteristic length obtained from the FE mesh size projected into the normal crack direction (mm); G_f is the fracture energy required to create a unit area of stress-free crack (N/mm); G_{f0} is the base value of fracture energy based on the maximum aggregate size of 16 mm (= 0.03 N/mm) [41]; c_1 and c_2 are empirical constants, and the values of $c_1 = 3$ and $c_2 = 6.93$ have been proposed based on available experimental data [40]. In this work, the concrete tensile strength used in the analysis was computed using Eq. (2b).

3.2 Shear Model

To represent the reduction in the shear modulus of the concrete after cracking, a shear retention factor following the expression proposed by Kolmar [42] was used (see Figure 4(b)). In this formulation, the shear modulus is related to the strain normal to the crack, ε_1, which is indicative of the crack opening [37]. The governing equations used to describe the shear retention factor are [37,42]:

$$G = r_g G_c \tag{3a}$$

$$r_g = c_3 \frac{-ln\left(\frac{1000\varepsilon_1}{c_1}\right)}{c_2} \tag{3b}$$

$$c_1 = 7 + 333(\rho - 0.005) \tag{3c}$$

$$c_2 = 10 - 167(\rho - 0.005) \; if \; 0 < \rho \leq 0.02 \tag{3d}$$

where G is the shear modulus after cracking (MPa); r_g is the shear retention factor; G_c is the initial shear modulus (MPa); c_1 and c_2 are parameters depending on the steel bar(s) crossing in the crack direction; ρ is the transformed reinforcing steel ratio to the crack plane; and c_3 is a user scaling factor (by default $c_3 = 1$). In this study, ρ was taken as zero so that the restraining effects from the reinforcing steel could be considered automatically in the analysis. Another way to compute the shear retention factor is by relating the post-cracking shear stiffness to the stiffness along the crack opening direction using a scaling factor [35,37,39]. The former approach was adopted in this paper.
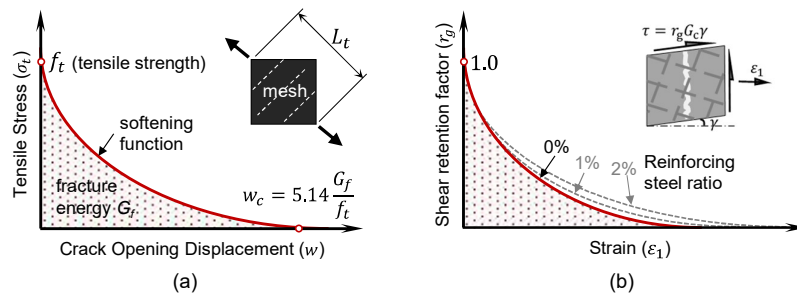

Figure 4 (a) Tension and (b) shear retention models for concrete [37].

Apart from the reduction in shear stiffness, it was assumed that the maximum shear stress, τ_{max}, that can be transmitted across a crack is related to the crack opening displacement, w, and the maximum aggregate size, a_g, as given by [43]:

$$\tau_{max} = \frac{0.18\sqrt{f'_c}}{0.31 \frac{24}{a_g+16}} \tag{4}$$

where f'_c is the concrete compressive strength (MPa).

In addition to the constitutive models described above, a reduction in concrete compressive strength due to transverse cracking was considered following the multi-linear model proposed in [15]. In this model, no reduction in compressive strength is considered when the tensile strain normal to a crack is less than 0.1%. Between 0.1% and 0.5%, the compressive strength is assumed to decrease linearly from 1.0 to 0.6; thereafter, a constant value of 0.6 is considered.

3.3 Reinforcement Model

Steel reinforcement in concrete can be modeled either in the form of smeared or discrete reinforcement. In the smeared representation, the reinforcement is distributed over the entire volume of an element and as such, the ratio of the total

area of the reinforcing bars along any direction to the area of the considered mesh must be inputted. In the discrete model, the reinforcement was treated as a one-dimensional truss element embedded inside the concrete. In either representation, specific stress-strain relations of the steel can be defined, including linear, bilinear, bilinear with hardening, or multilinear model.

In this study, the discrete model with multilinear stress-strain relation was used. The reinforcing steel was modeled using a truss element with axial stiffness only. In ATENA, the compatibility between the truss element representing the reinforcing bar and the solid element representing the concrete is achieved by imposing a kinematic constraint between the displacement at each nodal point of the truss element and the displacements of the nodal points of the solid element using an interpolation function [36,37]. In this work, the bond between concrete and steel was assumed to be in perfect condition (no bond-slip consideration).

Figure 5 presents a schematic of the stress-strain relation employed in this study. The yield and ultimate strengths for each steel bar (f_1 and f_4) were inputted from the values reported in the original experiment, while f_2 and f_3 were assumed based on the available data. The strain capacity of the reinforcing steel, ε_4, was taken as 0.1, which is a typical value used in non-seismic regions, whereas ε_2 and ε_3 were assumed as 0.02 and 0.05, respectively.
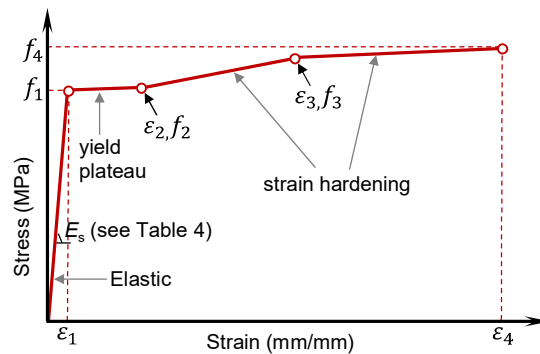

Figure 5   User-defined multilinear stress-strain relation for reinforcing steel [37].

3.4   Mesh and Boundary Conditions

All beams were modeled using an 8-node hexahedral (brick) linear element, with each node having x-, y- and z-translations. A typical mesh size of 0.05 m was used. The plates at the loading, support and anchor points were modeled using a tetrahedral linear element to prevent localized yielding. The geometry and dimensions of these plates were in accordance with those used in the experiment. Each beam was simply supported at the bottom as in the experiment.

An example of the finite element mesh used in the analysis is presented in Figure 6. The bottom longitudinal bars were extended past both ends of each beam and connected to a steel element representing the anchor plates as in the experiment. The analysis for each beam was run under a monotonically increasing displacement of 0.25 mm per step, until failure. At each displacement increment, the beam deflection at the bottom of the beam at midspan and the load acting on the top plate were monitored and compared with the experimental data reported in [27,28].
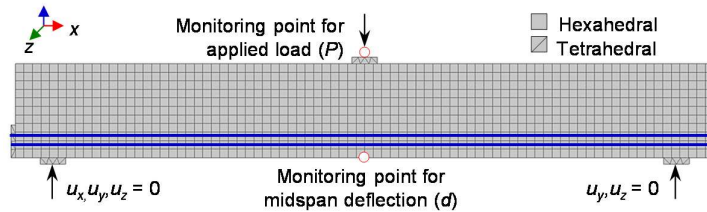

Figure 6 Typical finite element mesh and boundary conditions for beam OA1.

4 Results and Discussion

4.1 Response of Beam B1

To demonstrate the suitability of the models in predicting the nonlinear behavior of concrete in a shear-critical beam, Figure 7(a) presents the predicted load-deflection response of beam B1. This beam was specifically selected as it displays three different behavioral responses (flexure, shear, and compression), thereby providing a more comprehensive measure of the accuracy of the models. To describe the different behavioral responses, six stages of loading are highlighted in Figure 7(a) and discussed below.

The predicted maximum principal strains and crack patterns are plotted in the deformed state (magnified 5 times) in Figures 7(b)-(g) and for reasons of clarity, the experimental crack pattern at failure is displayed as an insert in Figure 7(a). In general terms, the response of the beam can be characterized as shear-compression in nature. With reference to Figure 7(b), the early stage of loading (50 kN) is shown to result in the formation of flexural cracks at the bottom of the beam and a subsequent increase in principal tensile strain.

As the load increases to 140 kN, new and pre-existing flexural cracks propagate upwards, thereby increasing the prominence of the strain bands (Figure 7(c)). As the load increases to 210 kN (Figure 7(d)), existing cracks propagate further upwards alongside with the strain bands, resulting in a fan-shaped pattern that

radiates from the load point. A highly localized strain is evident in the web region when the load reaches 290 kN (Figure 7(e)), which is indicative of the onset of critical shear cracking. This continues up to the peak load (429 kN; Figure 7(f)). Throughout this final stage of loading, the flexural cracks stop progressing and damage is concentrated mainly in the web region, indicating the behavioral change from flexural to critical shear.
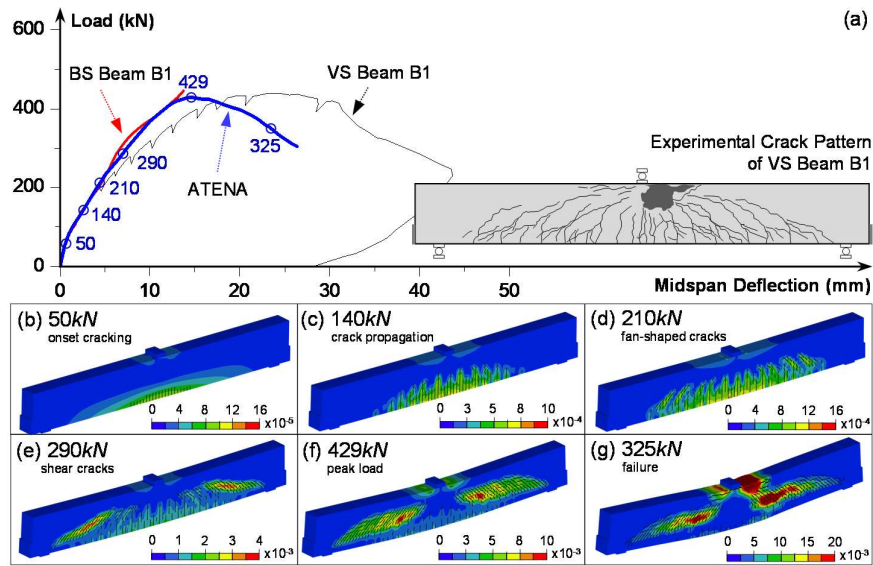

Figure 7   (a) Load-deflection response of beam B1; (b)-(g) principal tensile strain and crack patterns at selected key stages of loading.

Failure is predicted to occur due to crushing of the concrete at the top of the beam next to the loading plate (see Figure 7(g)), which is consistent with the experimental evidence. The response of the beam beyond the peak load is no longer symmetric, which can partly be attributed to the limitations in the iteration algorithm used. It is worth noting that this asymmetric response has no direct link with the non-symmetric crack pattern of beam B1 at failure, which occurred due to natural variations in material properties and/or possible (minor) errors in physical testing; their close resemblance is interesting however.

4.2   Comparison of Load-deflection Response

To further check the accuracy of the models presented in this paper, Figures 8(a)-(l) compare the predicted and observed load-deflection responses for all beams, together with predictions of the ACI 318M-14 design code equations [44] in terms of flexure and shear capacities, which are indicated in each figure with a

solid and dashed line, respectively. Each column presents the response of each series of beams with an identical cross-section but with different span lengths and reinforcement arrangements. The first and second columns display the results of notionally identical beams with and without transverse reinforcement, while the third and fourth columns display the results of companion beams with smaller widths (B and C series, respectively). The beam span increases from top-to-bottom: 3.66, 4.57, and 6.40 m. A summary of the predicted and observed load capacity and beam deflection for all VS beams (and their BS duplicates) is presented in Table 4.

With reference to Figures 8(a)-(l), it is evident that the predicted load-deflection responses displayed a reasonable agreement with the experimental data, considering the natural variations exhibited by the BS and VS beams. Each beam was predicted to display a linear response, followed by a transitional nonlinear response up to the peak. The predicted responses for beams with no transverse reinforcement (beams OA1, OA2, and OA3) exhibited stiffer post-peak responses than the VS beams, replicating more closely the overall stiffness of the BS beams (see Figures 8(a), (e) and (i)). A good agreement between the predicted and observed load capacities was produced, giving a mean ratio of experimental-to-predicted load capacity of 0.95/0.99 (based on the VS/BS beams) with a coefficient of variation (COV) of 5.0%/10.5% (VS/BS). It is noteworthy that, due to the absence of transverse reinforcement, a significant drop in load was apparent in all OA series beams immediately after attaining the peak load, highlighting the dangerous brittle mode of failure which beams without transverse reinforcement can exhibit.

From the comparison of the predicted and observed load-deflection responses of the beams with transverse reinforcement (A1-A3, B1-B3 and C1-C3), presented in Figures 8(b)-(d), (f)-(h) and (j)-(l), a similar trend in terms of the initial stiffness, peak load and maximum deflection can be observed. Slight variations are apparent in terms of the peak load and maximum deflection predictions, but they were all within a reasonable agreement and produced the same degree of accuracy as the analysis of the beams without transverse reinforcement discussed above. Of interest is the ability of the models to reproduce the more ductile response of the longer beams (i.e. A3, B3, and C3), as indicated by the plastic plateau in the load-deflection response.

The mean ratios of experimental-to-predicted load capacity for the beams with transverse reinforcement were 0.94/1.01 (based on VS/BS beams) with a COV of 3.7%/4.5% (VS/BS), highlighting once again the accuracy of the numerical predictions.
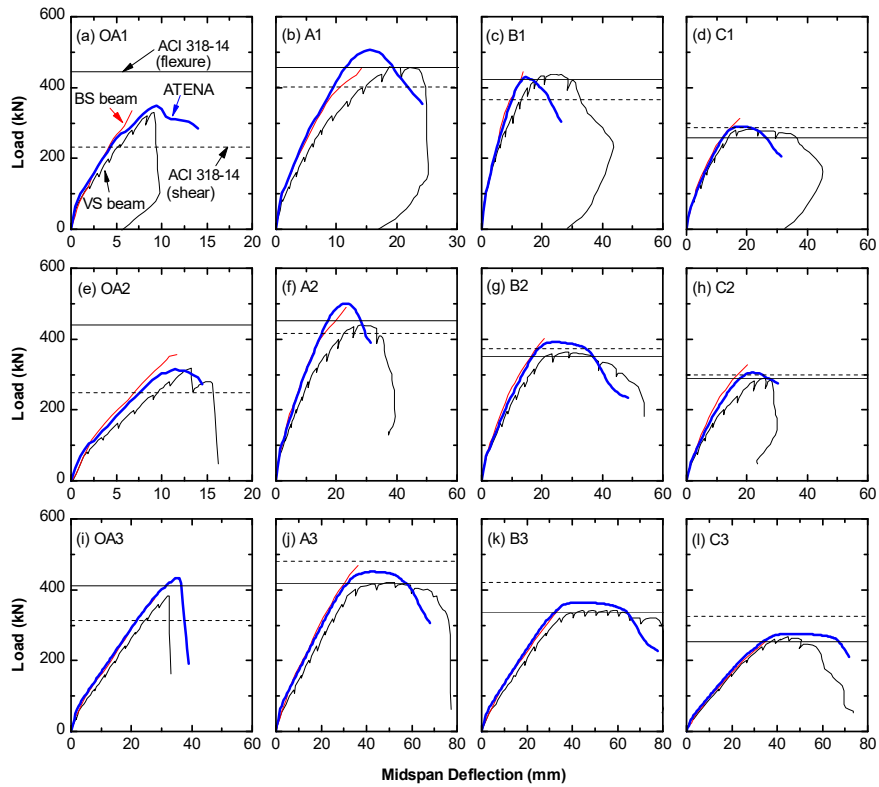
Figure 8 Predicted and observed load-deflection responses for all beams.

Table 4 Summary of predicted and observed load and deflection capacities for all beams (the number in brackets represents the value for BS beams).

Beam	Ultimate Load (kN)			Midspan Deflection (mm)		
	$P_{u\text{-Test}}$	$P_{u\text{-Calc}}$	$P_{u\text{-Test}}/P_{u\text{-Calc}}$	$\delta_{u\text{-Test}}$	$\delta_{u\text{-Calc}}$	$\delta_{u\text{-Test}}/\delta_{u\text{-Calc}}$
OA1	331 (334)	349 (349)	0.95 (0.96)	9.10 (6.6)	9.5 (9.5)	0.96 (0.69)
OA2	320 (356)	316 (316)	1.01 (1.13)	13.2 (11.7)	11.5 (11.5)	1.15 (1.02)
OA3	385 (378)	433 (433)	0.89 (0.87)	32.4 (27.9)	35.5 (35.5)	0.91 (0.79)
A1	459 (468)	506 (506)	0.91 (0.92)	18.8 (14.2)	15.5 (15.5)	1.21 (0.92)
A2	439 (490)	500 (500)	0.88 (0.98)	29.1 (22.9)	22.6 (22.6)	1.29 (1.01)
A3	420 (468)	458 (458)	0.92 (1.02)	51.0 (35.8)	42.2 (42.2)	1.21 (0.85)
B1	434 (446)	429 (429)	1.01 (1.04)	22.0 (13.7)	14.6 (14.6)	1.51 (0.94)
B2	365 (400)	391 (391)	0.93 (1.02)	31.6 (20.8)	23.7 (23.7)	1.33 (0.88)
B3	342 (356)	364 (364)	0.94 (0.98)	59.6 (35.3)	42.7 (42.7)	1.40 (0.83)
C1	282 (312)	290 (290)	0.97 (1.08)	21.0 (17.8)	18.7 (18.7)	1.12 (0.95)
C2	290 (324)	305 (305)	0.95 (1.06)	25.7 (20.1)	21.6 (21.6)	1.19 (0.93)
C3	265 (270)	275 (275)	0.96 (0.98)	44.3 (36.8)	47.3 (47.3)	0.94 (0.78)
		Mean	0.94 (1.00)		Mean	1.18 (0.88)
		COV (%)	4.10 (6.64)		COV (%)	17.67 (9.42)

Table 4 presents the mean ratios of experimental-to-predicted load capacity and maximum deflection. Overall, based on comparison with the twelve BS beams and their duplicates (VS beams), the models presented in this paper produced a mean observed-to-predicted load ratio of 0.94/1.00 (VS/BS) and a COV of only 4.1%/6.6% (VS/BS), which is better than the ACI predictions with a mean of 1.13/1.20 (VS/BS) and a COV of 12.68%/11.82% (VS/BS). It is worth noting that in ACI predictions, the predicted load is taken as the minimum of the load that corresponds to flexure and shear capacities. From Table 4, it is also evident that the beam deflection was less accurately predicted, producing a mean ratio of 1.18/0.88 (VS/BS) and a COV of 17.67%/9.42% (VS/BS). However, considering the natural variations across the tests, the nonlinear FE modeling presented in this paper could be regarded as sufficiently accurate. All parameters have also been applied to all beams in a consistent manner, thereby providing an objective measure of their accuracy.

4.3   Comparison of Crack Patterns

To provide further evidence of the accuracy of the models employed in this study, Figures 9 and 10 compare the observed failure crack patterns with the predicted maximum principal strains and crack patterns beyond the peak load. In general, there was a reasonably good agreement in the location and magnitude of cracking.
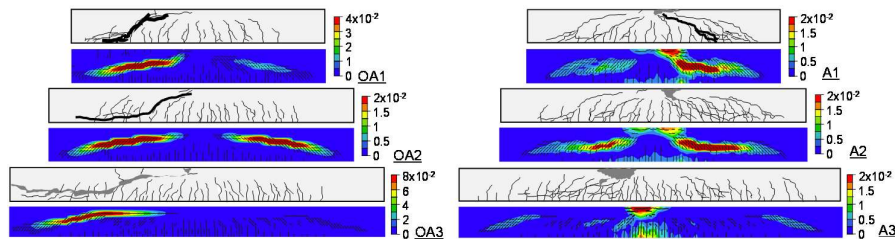

Figure 9   Predicted and observed failure crack patterns and maximum principal strains for the OA-series beams with no shear reinforcement and for the A-series replicate beams with shear reinforcement.
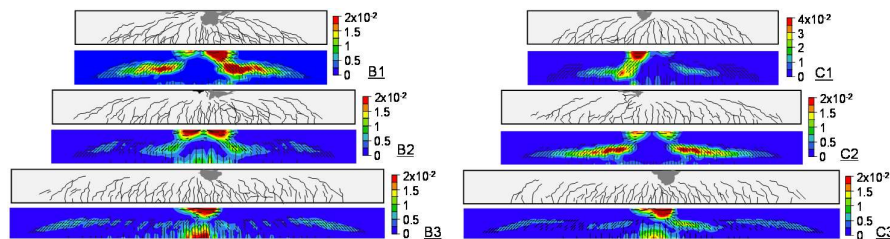

Figure 10   Predicted and observed failure crack patterns and maximum principal strains for the B- and C-series beams with shear reinforcement.

In the first three beams with no transverse reinforcement (OA series), the final failure was due to the sudden formation of diagonal tension cracking that continued as a horizontal crack to the beam end (see Figure 9). In the beams with transverse reinforcement, the mode of failure of the beams with short and intermediate spans (beams A1, A2, B1, B2, C1 and C2) can be described mainly as shear-compression in nature. In contrast, the mode of failure of the longest spanning beams (beams A3, B3 and C3) can be characterized as flexural-compression due to local crushing of the concrete in the compression zone. In beams with short and intermediate spans (series 1 and 2), severe diagonal cracks were found to develop in the later stages of loading and failure was ultimately triggered by crushing of the concrete in the flexural compression zone, which is consistent with experimental findings. The extent of the diagonal cracking in beams with a long span (series 3) was found to be less significant.

5   Concluding Remarks

This paper highlights the application of nonlinear finite element analysis to provide a critical assessment of the response of reinforced concrete beams in series of tests undertaken by Bresler-Scordelis (BS) and Vecchio-Shim (VS). Based on the work presented, the use of a smeared fixed crack approach in conjunction with fracture-plastic material models can provide accurate predictions of load and deflection capacities. A mean experimental-to-predicted load capacity of 0.94/1.00 (based on the VS/BS beams) and a COV of 4.1%/6.6% (also based on the VS/BS beams) were obtained. It was shown that in beams with no transverse reinforcement, failure was caused by sudden formation of diagonal-tension cracking, which in some cases were combined with horizontal splitting at either the support or point of load application. In beams with transverse reinforcement, both short and intermediate span beam series were predicted to exhibit shear-compression failure, while the long span beam series was predicted to display flexure-compression failure, which is consistent with the experimental findings.

The use of the analysis tool presented in this paper can provide practicing engineers with the ability to assess the response of structural elements in detail. The post-processing facilities can be particularly useful for assessing the behavior of a structural element with unusual and inadequate reinforcement detailing. Work in this direction is continuing.

Acknowledgements

References

[1]   Bae, B.I., Chung, J.H., Choi, H.K., Jung, H.S. & Choi, C.S., *Experimental Study on the Cyclic Behavior of Steel Fibre Reinforced High Strength Concrete Columns and Evaluation of Shear Strength*, Engineering Structures, **157**, pp. 250-267, 2018.

[2]   Ziara, M.M., Haldane, D. & Hood, S., *Proposed Changes to Flexural Design in BS 8110 to Allow Over-Reinforced Sections to Fail in a Ductile Manner*, Magazine of Concrete Research, **52**(6), pp. 443-454, 2000.

[3]   Duong, K.V., *Seismic Behaviour of Shear-critical Reinforced Concrete Frame: An Experimental and Numerical Investigation*, MASc Thesis, University of Toronto, 2006.

[4]   Sharma, A., Eligehausen, R. & Reddy, G.R., *A New Model to Simulate Joint Shear Behaviour of Poorly Detailed Beam-Column Connections in RC Structures under Seismic Loads, Part I: Exterior Joints*, Engineering Structures, **33**(3), pp. 1034-1051, 2011.

[5]   Collins, M.P., Bentz, E.C. & Sherwood, E.G., *Where is Shear Reinforcement Required? Review of Research Results and Design Procedures*, ACI Structural Journal, **105**(5), pp. 590-600, 2008.

[6]   Budiono, B., Dewi, H., Triani, N., Lim, E. & Sahadewa, A., *Finite Element Analysis of Reinforced Concrete Coupling Beams*, Journal of Engineering & Technological Sciences, **51**(6), pp. 762-771, 2019.

[7]   Pimanmas, A. & Maekawa, K., *Finite Element Analysis and Behaviour of Pre-cracked Reinforced Concrete Members in Shear*, Magazine of Concrete Research, **53**(4), pp. 263-282, 2001.

[8]   Suryanto, B., Nagai, K. & Maekawa, K., *Modeling and Analysis of Shear-critical ECC Members with Anisotropic Stress and Strain Fields*, Journal of Advanced Concrete Technology, **8**(2), pp. 239-258, 2010.

[9]   Bujadham, B. & Maekawa, K., *The Universal Model for Stress Transfer Across Cracks in Concrete*, Proceedings of JSCE, **451**(17), pp. 227-287, 1992.

[10]   Suryanto, B., Nagai, K. & Maekawa, K., *Smeared-crack Modeling of R/ECC Membranes Incorporating an Explicit Shear Transfer Model*, Journal of Advanced Concrete Technology, **8**(3), pp. 315-326, 2010.

[11]   Shima, H., Chou, L.L. & Okamura, H., *Micro and Macro Models for Bond in Reinforced Concrete*, Journal of the Faculty Engineering, **39**(2), pp. 133-194, 1987.

[12] Belarbi, A. & Hsu, T.T.C., *Constitutive Laws of Concrete in Tension and Reinforcing Bars Stiffened by Concrete*, ACI Structural Journal, **91**(4), pp. 465-474, 1994.

[13] Maekawa, K., Okamura, H. & Pimanmas, A., *Nonlinear Mechanics of Reinforced Concrete*, Spon Press, London, UK, 2003.

[14] FIB Bulletin No. 45, *Practitioners' Guide to Finite Element Modelling of Reinforced Concrete Structures*, State-of-Art Report, Jun. 2008.

[15] Tambusay, A., Suryanto, B. & Suprobo, P., *Visualization of Shear Cracks in a Reinforced Concrete Beam using the Digital Image Correlation*, International Journal on Advanced Science, Engineering and Information Technology, **8**(2), pp. 573-578, 2018.

[16] Feld, J. & Carper, K.L., *Construction Failure, Second Edition*, John Wiley & Sons, Inc., New York, US. 1996.

[17] Mitchell, D., Marchand, J., Croteau, P. & Cook, W.D., Concorde Overpass Collapse: Structural Aspects, **25**(6), pp. 545-553, 2011.

[18] Suryanto, B., Tambusay, A. & Suprobo, P., *Crack Mapping on Shear-critical Reinforced Concrete Beams using an Open Source Digital Image Correlation Software*, Civil Engineering Dimension, **19**(2), pp. 93-98, 2017.

[19] Suryanto, B., Morgan, R. & Han, A.L., *Predicting the Response of Shear-critical Reinforced Concrete Beams Using Response-2000 and SNI 2847:2013*, Civil Engineering Dimension, **18**(1), pp. 16-24, 2016.

[20] Ayoub, A. & Filippou, F.C., *Nonlinear Finite Element Analysis of Reinforced Concrete Shear Panels and Walls*, ASCE Journal of Structural Engineering, **124**(3), pp. 298-308, 1998.

[21] Chung, W. & Ahmad, S.H., *Analytical Model for Shear Critical Reinforced Concrete Members*, ASCE Journal of Structural Engineering, **121**(6), pp. 1023-1030, 1995.

[22] Dabbagh, H. & Foster, S.J., *A Smeared – Fixed Crack Model for FE Analysis of RC Membranes Incorporating Aggregate Interlock*, Advances in Structural Engineering, **9**(1), pp. 91-102, 2006.

[23] Vecchio, F.J., *Analysis of Shear-critical Reinforced Concrete Beams*, ACI Structural Journal, **97**(1), pp. 102-110, 2000.

[24] Vecchio, F.J. & Shim, W., *Experimental and Analytical Reexamination of Classic Concrete Beam Tests*, Journal of Structural Engineering, **130**(3), pp. 460-469, 2004.

[25] Bresler, B. & Scordelis, A., *Shear Strength of Reinforced Concrete Beams*, Journal of American Concrete Institute, **60**(1), pp. 51-72, 1963.

[26] Caresa, P. & Viquez, A.G., *Nonlinear Analysis of Shear Critical RC Members using Current FE Software*, 6th ECCOMAS Thematic Conference on Computational Methods in Structural Dynamics and Earthquake Engineering, Greece, Jun. 2017.

[27]   Ma, R.L., *Program Sherlock: A Tool for Stochastic Finite Element Analysis and Field Assessment of Concrete Structures*, MASc Thesis, University of Toronto, Canada, 2018.

[28]   Bernard, S., Finite Element Modelling of Reinforced Concrete Beams with Corroded Shear Reinforcement, MASc Thesis, University of Ottawa, Canada, 2013.

[29]   Červenka Consulting, *ATENA for Non-linear Finite Element Analysis of Reinforced Concrete Structures*, https://www.cervenka.cz/company/ (April 2020)

[30]   Tambusay, A. & Suprobo, P., *Predicting the Flexural Response of a Reinforced Concrete Beam using the Fracture-Plastic Model*, Journal of Civil Engineering, **34**(2), pp. 61-67, 2019.

[31]   Červenka, V., Červenka, J., Pukl, R. & Sajdlova, T., *Prediction of Shear Failure of Large Beam Based on Fracture Mechanics*, 9th International Conference on Fracture Mechanics of Concrete and Concrete Structures (FraMCoS-9), 2016.

[32]   Don, W., Chong, K., Aitken, M., Tambusay, A., Suryanto, B. & Suprobo, P., *Influence of Link Spacing on Concrete Shear Capacity: Experimental Investigations and Finite Element Studies*, IOP Conference Series: Materials Science and Engineering, **930**(1), 012052, 2020.

[33]   Kadlec, L. & Červenka, V., *Uncertainty of Numerical Models for Punching Resistance of RC Slabs*, FIB Symposium Copenhagen, Denmark, 2015.

[34]   Tambusay, A., Suryanto, B. & Suprobo, P., *Nonlinear Finite Element Analysis of Reinforced Concrete Beam-Column Joints Under Reversed Cyclic Loading*, IOP Conference Series: Materials Science and Engineering, **930**(1), 012055, 2020

[35]   Hajkova, K., Smilauer, V., Jendele, L. & Červenka, J., *Prediction of Reinforcement Corrosion due to Chloride Ingress and Its Effects on Serviceability*, Engineering Structures, **174**(1), pp. 768-777, 2018.

[36]   Jendele, L. & Červenka, J., *On the Solution of Multi-Point Constraints – Application to FE Analysis of Reinforced Concrete Structures*, Computers & Structures, **87**(15-16), pp. 970-980, 2009.

[37]   Červenka, V., Jendele, L. & Červenka, J., *ATENA Program Documentation – Part 1: Theory, Červenka Consulting*, Prague, December 3, 2018.

[38]   Menétrey, P. & Willam, K.J., *Triaxial Failure Criterion for Concrete and Its Generalization*, ACI Structural Journal, **95**(3), pp. 311-318, 1995.

[39]   Červenka, J., Červenka, V. & Laserna, S., *On Crack Band Model in Finite Element Analysis of Concrete Fracture in Engineering Practice*, Engineering Fracture Mechanics, **197**, pp. 27-47, 2018.

[40]   Hordijk, D.A., *Local Approach to Fatigue of Concrete*, PhD dissertation, Delft University of Technology, 1991.

[41] CEB-FIP, *Comité Euro-International du Béton (CEB-FIP Model Code 1990)*, Information Bulletin, 195, 1990.

[42] Kolmar, W., *Beschreibung der Kraftuebertragung Über Risse in Nichtlinearen Finite-Element-Berechnungen von Stahlbetontragwerken*, PhD Thesis, Darmstadt University of Technology, Germany, 1986.

[43] Vecchio, F.J. & Collins M.P., *Modified Compression-Field Theory for Reinforced Concrete Beams Subjected to Shear*, ACI Journal, **83**(2), pp. 219-231, 1986.

[44] ACI 318M-14, *Building Code Requirements for Structural Concrete and Commentary*, American Concrete Institute, 2014.